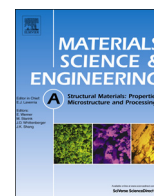




ELSEVIER

Contents lists available at ScienceDirect

## Materials Science &amp; Engineering A

journal homepage: [www.elsevier.com/locate/msea](http://www.elsevier.com/locate/msea)

# Metallic sandwiches with open porosity facings and closed porosity cores for SOFC interconnects

Justin A. Scott<sup>1</sup>, David C. Dunand\*

Department of Materials Science and Engineering, Northwestern University, Evanston, IL 60208, USA

## ARTICLE INFO

## Article history:

Received 6 January 2013

Received in revised form

21 June 2013

Accepted 24 June 2013

Available online 20 July 2013

## Keywords:

Ferritic steels

Nickel alloys

Fuel cells

Porous materials

Mechanical characterization

Powder metallurgy

## ABSTRACT

Iron- and nickel-based sandwich structures with open porosity facings and closed-porosity cores were created by melt infiltration and powder metallurgy, respectively, for application as interconnects in high-temperature fuel cells. For E-Brite (Fe–Cr–Mo) sandwiches, open porosity faces were created by evaporation of NaCl particles mixed with the metallic powders, while closed porosity in the core resulted from partial sintering of the pure metallic powders. Sandwiches from J5 (Ni–Mo–Cr–Ti–Mn–Al–Y) were produced by infiltrating the liquid alloy into a sandwich scaffold of permanent Al<sub>2</sub>O<sub>3</sub> hollow spheres in the core and leachable NaAlO<sub>2</sub> particles in the facings. Mechanical properties of both sandwich types were measured in three-point bending and indicated similar modes of failure by face yielding. Stiffness measurements closely match model values for E-Brite sandwiches but are below expected values for J5 sandwiches. In the case of sandwich yield load, calculated values for E-Brite slightly underestimated experimental values, while J5 experimental performance was significantly overestimated.

© 2013 Elsevier B.V. All rights reserved.

## 1. Introduction

Metallic foams display many properties that make them attractive for use in lightweight structural applications [1–3]. Their combination of low density, high energy absorption, and high specific strength and stiffness make them well-suited as elements for sandwich panels [4–6]. Metallic foams are typically employed as the core layer sandwiched between two thin, dense alloy sheets [7]. Mechanically, this configuration can offer significant benefits for weight-optimized bending stiffness [8–12] and, in some cases, even yield-limited design as demonstrated with functionally graded Al-based foams [13,14]. To date, however, fully porous sandwiches, with open-porosity facings sandwiching a closed-porosity core, have not been studied, neither in terms of fabrication methods nor mechanical properties.

Planar solid-oxide fuel cells (SOFC) are typically connected in series into stacks, with interconnects providing electrical connectivity across cells and physical separation between the fuel at the anode-side of one cell from the air at the cathode-side of the adjacent cell. One of the most common interconnect designs consists of a conductive metallic plate with channels on each side

of the bipolar plate to allow for gas flow [15–18]. Some recent designs for SOFC interconnects utilize a sandwich structure with thick, open-porosity facings and a thin, pore-free core [19–21]. In this lightweight interconnect architecture, which is especially advantageous for mobile SOFCs applications, the open pores in the facings can serve as fluid channels for fuel and oxidant across the electrodes while the dense, pore-free core acts as a physical barrier between them [18]. It is also possible for the core of the interconnect sandwich to be a closed-porosity or syntactic foam layer instead of a pore-free material, which enables meeting the minimum strength and stiffness requirement of the interconnect with less weight/material. Since SOFCs operate at high temperature (typically at 700–800 °C), Fe-based chromia-forming alloys (i.e., ferritic alloys) are commonly considered the best candidate materials for SOFC interconnects due to their high oxide conductivity compared to alternative alumina- and silica-forming iron-based alloys [16].

Though less prominent in the literature, Ni-based alloys are also considered suitable for SOFC interconnects. While their coefficient of thermal expansion is not as well matched with ceramic SOFC components compared to ferritic steels, they offer better mechanical strength, which is advantageous in auxiliary power units for mobile applications where stacks may be subject to impact and vibrations. As only a few Ni-based alloys have been studied for SOFC applications, mostly in bulk form, limited information is available on the properties of porous Ni-based foams for SOFCs. Here, a replicated J5 foam studied previously

\* Corresponding author. Tel.: +1 847 491 5370; fax: +1 847 467 6573.

E-mail addresses: [jscott@u.northwestern.edu](mailto:jscott@u.northwestern.edu) (J.A. Scott), [dunand@northwestern.edu](mailto:dunand@northwestern.edu) (D.C. Dunand).<sup>1</sup> Present Address: The Minerals, Metals & Materials Society, 184 Thorn Hill Road, Warrendale, PA, 15086-7514, USA.

[22,23] is used for the facings while a thermoreversible gelcasting (TRG) technique is employed to create a syntactic foam core with J5 and hollow alumina spheres. TRG involves the formation of a reversible, physically cross-linked polymer gel that, after cooling to room temperature, can be reheated and re-casted. The process is well suited for complex shapes and the high aspect ratios of components in SOFC systems [24].

Here, we describe two new methods, based on casting (for a Ni-based alloy) and powder metallurgy (for a ferritic steel), to create light-weight sandwiches with a novel, fully porous structure: open porosity facings and closed porosity cores. Despite the critical importance of preventing deformation of interconnects in the performance of SOFC, there is a paucity of data on the subject of flexural properties. We thus examine the flexural properties of these sandwich beams with thicknesses relevant to SOFC interconnects. A better understanding of the bending behavior is expected to influence the design of the stack and help determine the limitations of mechanical loading in mobile applications.

## 2. Experimental procedures

### 2.1. Processing

Sandwich structures were created using two alloys designed for SOFC interconnects: E-Brite (Fe–26Cr–1Mo, wt%) and J5 (Ni–22.5Mo–12.5Cr–1Ti–0.5Mn–0.1Al–0.1Y, wt%). For both alloys, sandwiches used for mechanical testing consisted of facings with open porosity of ~50% surrounding a closed-porosity core.

#### 2.1.1. E-Brite sandwiches

E-Brite sandwiches were prepared using a powder metallurgy approach. Two batches of powder blends were prepared, similar to the methods described in Ref. [25]. Type E1 consisted of elemental Fe (APS 6–10  $\mu\text{m}$ , 99.5% purity), Cr (APS < 10  $\mu\text{m}$ , 99.8% purity), and Mo (APS 3–7  $\mu\text{m}$ , 99.95% purity) acquired from Alfa Aesar (Ward Hill, MA). Powders were mixed in proportions corresponding to the E-Brite composition and blended with 50 vol% NaCl place-holder powders (crushed and sieved to 53–106  $\mu\text{m}$ ) to be used for producing the facings. For type E2, the elemental powders were mixed but no NaCl place-holder was added to create a denser core. A thin layer of E1 powders was poured into a 27.9 mm diameter steel die, spread flat, and hand-pressed with a steel punch to a height of ~0.6 mm. A second layer of E2 powders was added, spread flat, and hand-pressed with the punch as before, to a height of ~0.6 mm. A third layer of E1 powders (with the same mass as the first one) was poured, spread flat, and the entire compact was cold pressed at 350 MPa. The resulting compact was vacuum sintered at 1250 °C for 4 h, resulting in evaporation of the NaCl place-holder along with densification and interdiffusion of the metallic powders, as previously reported in Ref. [25].

Porosity of the facing was determined by Archimedes density measurements performed with water as the medium on a sample prepared solely with E1 powders, pressed and sintered under the same conditions as the sandwiches. Similarly, closed porosity of the E-Brite core was calculated by taking Archimedes density measurements in water on a separate sample prepared with only E2 powders. The same E-Brite bulk density of 7.7 g/cm<sup>3</sup> for E-Brite [26] was used in both cases.

#### 2.1.2. J5 sandwiches

Sandwich structures of J5 alloy were produced by infiltrating with liquid J5 a scaffold containing three layers with two types of place-holders.

The core, (J1), was first created via thermoreversible gelcasting (TRG) to obtain a flat beam that served as a permanent core

scaffold. For this step, as-received hollow alumina spheres (ALODUR KKW, < 500  $\mu\text{m}$ , 98 wt% Al<sub>2</sub>O<sub>3</sub>; Treibacher Schleifmittel; Andersonville, GA) were sieved, retaining those in the range 355–500  $\mu\text{m}$ . These hollow alumina spheres were further sorted by suspension in chloroform. Since chloroform has a higher density (1.48 g/cm<sup>-3</sup>) than the closed, hollow alumina spheres of the desired size (< 1.40 g/cm<sup>-3</sup>), these raised to the surface, while open spheres and fragments settled to the bottom of the beaker. The closed alumina spheres retrieved from the surface were rinsed with acetone and dried before further processing. A TRG system was subsequently produced with 6.7 wt% triblock copolymer, poly(methyl methacrylate)–poly(*n*-butyl acrylate)–poly(methyl methacrylate) (PMMA–PnBA–PMMA; 9k–53k–9k g mol<sup>-1</sup>; Kuraray, Japan) dissolved in 2-propanol, which preferentially solvated the PnBA midblock [24]. The mixture was sealed in a glass vial and sonicated in water heated to ~60–70 °C until the solution appeared a homogenous cloudy white indicating the transition to a low-viscosity solution via dissociation of the polymer end-blocks [27,28]. Solids, consisting of presorted, hollow alumina spheres (as described above) and alumina powders (0.36  $\mu\text{m}$  median particle size; Baikowski Malakoff, Inc.; Malakoff, TX) in a ratio of 20:1 by volume, was then dispersed in the solution in two batches about 5 min apart. Finally, a small amount (< 1 cc) of Aerosol AY-65 (Cytec; West Patterson, NJ) dispersant was added to stabilize the slurry. The warm slurry was then cast onto glass slides into circular steel washers (35 mm diameter opening, 1 mm thick) that were lubricated with vacuum grease. A second glass slide was placed on top of the washer and pressed down lightly to prevent cracking any of the hollow alumina spheres while flattening the slurry. Gelation rapidly occurred during cooling and the castings were further allowed to dry for 24 h in a fume hood. The cylindrical samples were then demolded and cut into ~10 × 30 mm<sup>2</sup> rectangles, which were heated (7 °C/min) in a vacuum furnace (~1 × 10<sup>-6</sup> Torr) for 1 h at 600 °C (to achieve copolymer burnout) and 1 h at 1525 °C (for sintering) before being furnace cooled.

The second type of placeholder used for faces (J2), consisted of sodium aluminate (NaAlO<sub>2</sub>) powders (~45 mesh; Alfa Aesar; Ward Hill, MA), which were prepared similarly to a method outlined previously [22,23]. Since the as-received powders were too fine for this study, they were cold-pressed at 350 MPa and fired at 1500 °C for 1 h in air before crushing and sieving to the range of 355–500  $\mu\text{m}$ .

With their longest dimension remaining vertical, three sintered J1 cores were placed upright in a 25 mm diameter alumina crucible, parallel to each other and each separated by a 5 mm gap. These beams formed the cores of three sandwich structures. Sodium aluminate powders were then poured in the remainder of the crucible to the height of the vertical beams filling the space between the cores and creating a preform filling the crucible. An ingot of J5 alloy, provided by the National Energy Technology Laboratory (Albany, OR) and sectioned into cubes of ~1 mm<sup>3</sup>, was placed on top of the preform but separated by a 3 mm thick alumina disc spacer to prevent possible reaction between J5 and place-holders during heating. The crucible was heated at 7 °C/min in vacuum (~1 × 10<sup>-6</sup> Torr) to 1450 °C and maintained for 1 h at this temperature to ensure complete melting of the J5 ingot. Argon was then introduced to the system to a pressure of 80 kPa and the pressure was maintained for 3 min, causing the melt to flow through the gap between the crucible wall and the spacer and infiltrate the pores of the preform. The ingot was subsequently furnace cooled while maintaining the pressurized argon for 1 h, ensuring that solidification occurred under pressure.

The infiltrated composite was cut into three sections with a high-speed diamond saw, each containing a J1 core surrounded by J2 facing materials (infiltrated sodium aluminate). Further cutting

and polishing produced three sandwiches, with J2 facing thickness of  $\sim 0.45$  mm and J1 core thicknesses of  $\sim 1.30$  mm each (i.e., a total specimen thickness of  $\sim 2.20$  mm). Sodium aluminate was subsequently removed from the facings of each of the sectioned samples by placing them in an aqueous 10% HCl solution under sonication for 24 h. Sodium aluminate, which is known to dissolve much more rapidly than J5 in 10% HCl [22], was completely removed with negligible removal of the surrounding matrix.

Due to the formation of second-phase precipitates in J5 [29], a heat treatment was performed, as used in previous work with this alloy for SOFC interconnects [22]. Sectioned specimens were solutionized at  $1100^\circ\text{C}$  for 4 h under argon and then aged at  $800^\circ\text{C}$  for an additional 4 h under argon, with water quenching at the termination of each step.

Porosity of the facing was determined by Archimedes density measurements on a J5 foam replicated from only sodium aluminate place-holders, which was cut from the bulk specimen, using a bulk density of  $8.6\text{ g/cm}^3$  for J5 [22]. Density of the closed-porosity core was found using the Archimedes method on a sample consisting solely of the syntactic foam material.

## 2.2. Mechanical properties

E-Brite and J5 samples were machined by diamond saw to a geometry consistent with the non-standard configurations of ASTM 7249 [30] but total thickness of all samples was chosen to be  $< 3$  mm to represent typical sizes for metal-supported SOFC interconnects [19,31]. Table 1 lists the dimensions of the samples tested in this study, with core and facing thicknesses representing an average value as obtained by optical microscopy observations at five locations on each of the two sides of the sample. If variance of a facing exceeded the average by 0.05 mm, the sample was rejected or further machined or polished until all dimension requirements were met. Every tested sample was polished to a minimum 1200 grit finish but selected specimens were further

**Table 1**

Dimensions of sandwiches tested in bending (see Fig. 1). Relative density is calculated by taking the gravimetric density of the beam (using dimensions to estimate its volume) and dividing it by the estimated density of a non-porous beam of the same alloy and volume.

Sample	$t_f$ [mm]	$t_c$ [mm]	$t_f/t_c$	$t$ [mm]	$b$ [mm]	$L$ [mm]	Rel. density [%]
EB-1	0.41	0.61	0.67	1.42	3.96	21.71	72
EB-2	0.45	0.66	0.68	1.56	3.98	22.36	71
EB-3	0.47	0.60	0.78	1.54	3.99	23.00	68
EB-4	0.47	0.58	0.81	1.52	3.99	21.64	68
EB-5	0.50	0.60	0.83	1.59	3.86	22.26	67
EB-6	0.48	0.57	0.84	1.53	4.00	22.98	67
EB-7	0.50	0.55	0.91	1.55	4.00	22.27	61
J5-1	0.42	1.33	0.32	2.19	4.49	20.01	49
J5-2	0.47	1.27	0.37	2.21	4.46	20.95	49

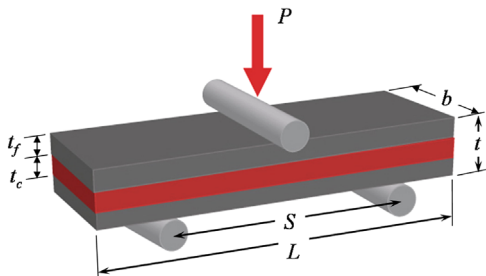


**Fig. 1.** Schematic of experimental three-point bend testing setup, with sample dimensions.

polished to  $0.05\ \mu\text{m}$  using an alumina slurry to facilitate post-testing investigation of bending failure.

Room-temperature three-point bending tests were performed on both types of sandwich structures using the loading configuration shown in Fig. 1. Loads were applied directly to samples via 5 mm diameter rollers in a MTS Sintech 20/G screw-driven load frame equipped with a 200 N load cell. A cross-head speed of  $0.3\text{ mm/min}$  was chosen to ensure failure within 3–6 min as specified in the standard used. Span length,  $S$ , was 16 mm in the case of E-Brite and 18 mm for J5 sandwiches. A very stiff A36 steel beam (25 mm in thickness) was tested in the loading train prior to sandwich testing to obtain overall machine compliance, which was later subtracted from the E-Brite and J5 sandwich deflection.

## 3. Results and discussion

### 3.1. Microstructural characterization

#### 3.1.1. E-Brite sandwich structures

Micrographs of the NaCl placeholder and sintered E-Brite specimens can be seen in Fig. 2. The angular characteristics of the salt powders are retained in the facing layers as previously reported [25]. The facing layer had a relative density of 50.4% as measured by the Archimedes method and the core layer had a relative density of 93.1%. This 6.9% porosity is well below the anticipated percolation limit of  $\sim 20\%$  and can thus be safely assumed to be closed, insuring that the core prevents mixing of gases present in the two faces when the sandwich is used as a SOFC interconnect. Using a thickness of 0.5 mm for both faces and cores, the relative density of the sandwich is calculated as 65%, with respect to the density of pore-free E-Brite of  $7.7\text{ g/cm}^3$ .

Good flatness of the interfaces between core and faces is also apparent in Fig. 2. Despite the high aspect ratio required ( $L/T \sim 15$ ), the powder metallurgy method developed here appears well

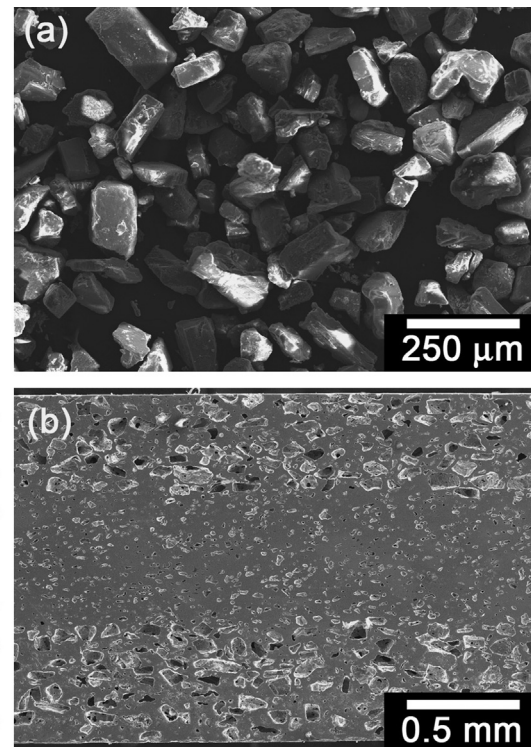


**Fig. 2.** SEM micrographs of (a) crushed NaCl placeholder after sieving and (b) polished edge of E-Brite sandwich beam, with thickness of facings ( $t_f$ ) and core ( $t_c$ ) identified.

suiting for providing a high degree of precision for tight interface tolerances.

### 3.1.2. J5 sandwich structures

Fig. 3 displays both types of place-holders used in the creation of J5 sandwich structures. Fig. 3a shows the sintered and sieved  $\text{NaAlO}_2$  powders, whose fine porosity (shown in inset) was not infiltrated by the melt, so that only the rough envelopes of the powders are replicated within the sandwich faces, as seen in Fig. 3c. A face average density of  $4.1 \text{ g/cm}^3$  was determined by Archimedes measurements, corresponding to a relative density of 48%. The face thickness of  $\sim 0.4 \text{ mm}$  allowed for only one  $\text{NaAlO}_2$  powder, on average.

After gel-casting and sintering, the alumina hollow spheres are connected by bridges created by sintering of the fine alumina powder (as visible in Fig. 3b). The core thickness of 1.3 mm is sufficient to encompass about three alumina hollow spheres, as illustrated in Fig. 3c, and the core is thus thick enough to prevent gas transfer from one facing to the other. The density of the core,

as determined by Archimedes measurements, was  $4.3 \text{ g/cm}^3$ , corresponding to a relative density of 50%. Based on a thickness of 0.4 mm for each face and a core thickness of 1.3 mm, the relative density of the sandwich is calculated as 49%.

Despite the relatively large  $355\text{--}500 \mu\text{m}$  size of the hollow spheres, interface flatness between core and facings was good in the case of J5 beams (Fig. 3c). Preliminary infiltration attempts utilizing packed layers of non-gelcasted, unsintered hollow alumina spheres and  $\text{NaAlO}_2$  were unsuccessful. No well-defined core/facing interface could be achieved because buoyancy forces on the low density hollow alumina spheres caused layer mixing.

### 3.2. Bending behavior

Bend testing was performed on seven E-Brite specimens and two J5 specimens that met the geometry specifications for non-standard configurations of ASTM 7249 [30] (see Table 1).

Fig. 4 displays curves of force/width ratio vs. displacement for the E-Brite sandwiches; although there is some variance in the maximum deflection at similar normalized loadings, the general trends are quite repeatable. Initially, a linear regime of elastic deformation is visible, followed by gradual deviation to non-linear loading with increasing load (i.e., plasticity). The flow curves do not appear to depend strongly on  $t_f$  or the ratio  $t_f/t_c$  as seen in Fig. 4. The peak normalized forces of all seven samples fall between 26 and 31 N/mm, corresponding to a difference of  $<20\%$  among any two beams, which indicates a good degree of reproducibility, especially given the variations in core and facing thicknesses (Table 1).

Beginning at a deflection of 0.6–1 mm, all beams showed signs of damage as one (or in some cases, two) cracks formed at the base (i.e., the tensile face) of the beam almost directly under the central loading roller. In all cases, cracks grew in the direction of the applied load and resulted in decreasing load with increasing deformation, visible as the long decline beyond the peak load in the curves in Fig. 4. When the crack reached the core layer, a change in behavior was observed: further deflection of the beam resulted in essentially flat loading or, in some cases, an increase in load. This behavior is expected, given the higher flow stress and crack resistance of the core. To confirm this behavior, one test was interrupted at this stage of deformation, immediately following a flattening of the load. The corresponding SEM micrograph in Fig. 5 confirms that the crack was located at the core-facing interface as anticipated. In the remaining tests, as the deflection increased and the crack propagated through the core, a concurrent, steady decrease in load was witnessed for all E-Brite beams.

Similar trends were observed in the force–displacement curves for the two J5 sandwiches, as depicted in Fig. 6. Again,

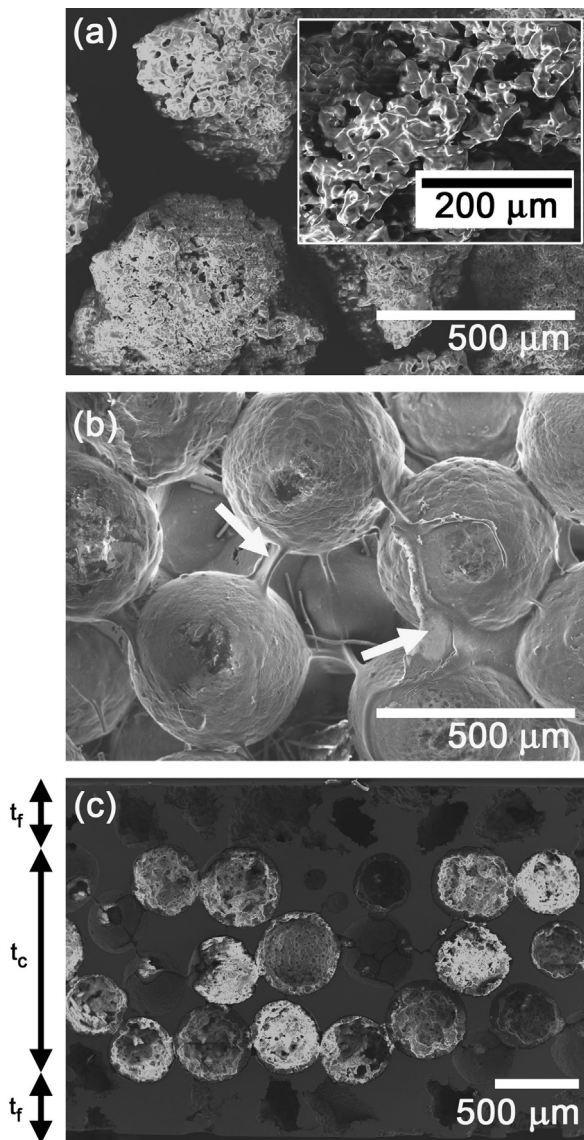


Fig. 3. SEM micrographs of (a) sieved  $\text{NaAlO}_2$  place-holders; (b) gelcast and sintered hollow alumina spheres with sintered necks highlighted by arrows; and (c) polished edge of J5 sandwich beam, with thickness of facings ( $t_f$ ) and core ( $t_c$ ) identified. Some of the alumina hollow spheres (white in micrograph) were pulled out from the core during metallographic preparation.

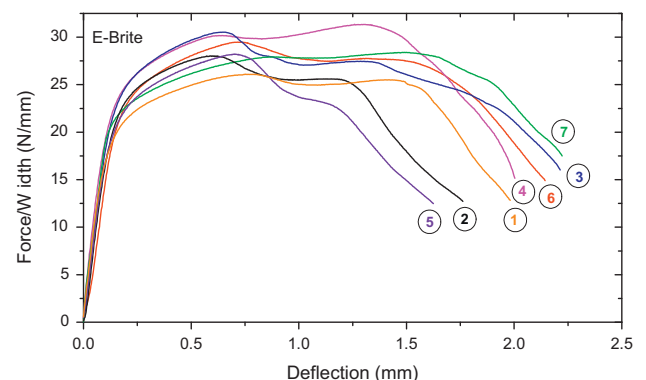
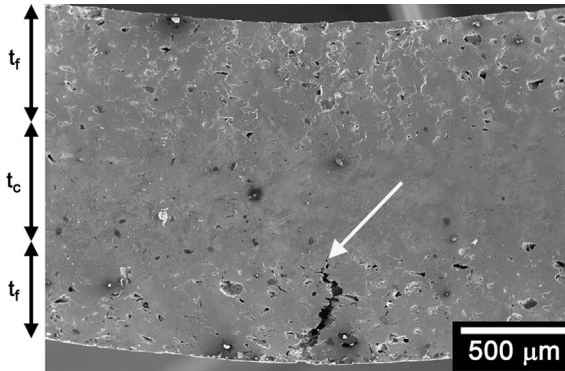


Fig. 4. Force–displacement curves for E-Brite sandwiches normalized by beam width. Ratio of face thickness to core thickness,  $t_f/t_c$ , increases with sample number.

linear-elastic deformation preceded a plastic flow region leading to a peak load. Just before this point was reached, serrations in the plot were observed, which likely correspond to fracture of struts in the facing and/or cracking of the alumina place-holders. Regardless of the mechanism, the relative size of place-holders resulted in each event having a large impact on the curve and their eventual accumulation led to a decrease in the load. A prolonged region of decreasing load occurs from 0.72 to 0.62 mm through completion of the test for J5-1 and J5-2, respectively. After some additional deflection, the curves begin to level, indicating the crack has reached the core. Further deformation results in decreasing loads and continued serrations, likely caused by the cracking of hollow alumina spheres as seen in the SEM micrograph of Fig. 7c and d. Also visible in the figure are the large deflections of the crack, likely due to its propagation around the large, stiff alumina spheres.

SEM observations of deformed E-Brite beams, such as in Fig. 7a and b, confirm that face yielding is the dominant mechanism of failure. Ductile failure of the matrix was evidenced in the dimpled surface of the crack. In the case of J5 beams, face yielding was also apparent, with the crack opening located just off center from the top loading roller. In the instance shown in Fig. 7c and d, the crack appears to have been deflected by the alumina microspheres, but it ultimately propagated towards the top loading roller. Continued crack growth through the core also resulted in cracked hollow alumina spheres as highlighted in the magnified micrograph Fig. 7d. Further inspection of both beam types in the SEM did



**Fig. 5.** SEM micrograph of E-Brite beam after bend testing was stopped immediately following the first visible peak load. At this point, the crack has propagated through the facing but the crack tip is located at the interface of the core and facing. White arrow indicates location where crack stopped, with thickness of facings ( $t_f$ ) and core ( $t_c$ ) identified at edge of image.

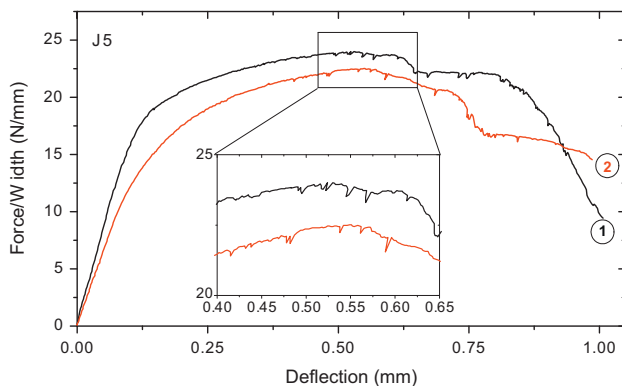


**Fig. 6.** Force–displacement curves for J5 sandwiches normalized by beam width. Inset displays a magnified view of region near peak stress showing serrations.

not reveal visible plastic deformation where the roller contacted the beam, thus indicating lack of facing indentation, which is another possible failure mechanism [32].

### 3.3. Modeling of bending behavior

#### 3.3.1. Stiffness

All beams displayed a linear regime of deformation at small deflections corresponding to the elastic regime. In this region, the stiffness, or rigidity, of the beam is defined as the ratio of the load,  $P$ , to the deflection,  $\delta$ . For the case of structural sandwiches with thick faces in three-point bending, the stiffness can be described by [33]:

$$\frac{P}{\delta} = \left[ \left( \frac{2S^3}{48E_f^*bt_f(t_c + t_f)^2} \right) + \left( \frac{St_c}{C_G4b(\rho_c^*/\rho_s)^2E_c^*(t_c + t_f)^2} \right) \right]^{-1} \quad (1)$$

In this equation,  $b$ ,  $S$ ,  $t_f$  and  $t_c$  are the sample dimensions shown in Fig. 1,  $E_f^*$  is Young's modulus of the facing,  $E_c^*$  is Young's modulus of the closed-porosity core,  $\rho_c^*/\rho_s$  is the relative density of the core, and  $C_G$  is a constant of proportionality between the relative shear modulus and relative density assumed here to be  $\approx 3/8$  as in Ref. [2]. Young's moduli of the facings and core, which are porous for the present sandwiches, are found using the Gibson–Ashby relation [2]:

$$E_{f,c}^* = C_E E_s \left( \frac{\rho_{f,c}^*}{\rho_s} \right)^2 \quad (2)$$

where the subscripts  $f$  and  $c$  are for the facings and the core respectively,  $E_s$  is Young's modulus of the bulk material,  $\rho^*/\rho_s$  is the relative density of the foams, and  $C_E$  is a scaling factor close to unity. Values employed for stiffness calculations are summarized in Table 2.

Stiffness values for both sandwich types calculated from Eqs. (1) and (2) are listed in Table 3 alongside experimental values obtained by determination of the slope in the linear regime. Correlated error was determined by taking the standard deviation of face thickness, core thickness, width and span measurements and subsequently propagating through Eq. (1). The primary contributions to uncertainty were from relative density as well as face and core thickness measurements. For the most part, experimental values of E-Brite beams were within the range of uncertainty of calculated values. In the case of J5 beams, however, experimental values were lower than those predicted by Eq. (1). This may be caused by the presence of deformation beyond what is predicted by the beam-theory derived from Eq. (1), similar to the behavior in graded Al foam beams reported by Pollien et al. [14]. In this case, the J5 core was strengthened by a network of hollow alumina spheres, thus it is possible that additional elastic deformation occurred in the faces in the loading direction during the experiment.

#### 3.3.2. Yield strength

The onset of face yielding occurs when the equivalent (normal) stress in the bottommost fiber matches the tensile yield stress of the facing. The yielding load,  $P_y$ , can then be calculated as [34]

$$P_y = \frac{4D}{S(t_c/2 + t_f)} \sigma_{fy}^* \quad (3)$$

where  $\sigma_{fy}^*$  is the yield stress of the foam facing and  $D$  is the flexural rigidity given by

$$D = E_f^* \frac{bt_f^3}{6} + E_f^* \frac{bt_f(t_f + t_c)^2}{2} + E_c^* \frac{bt_c^3}{12} \quad (4)$$

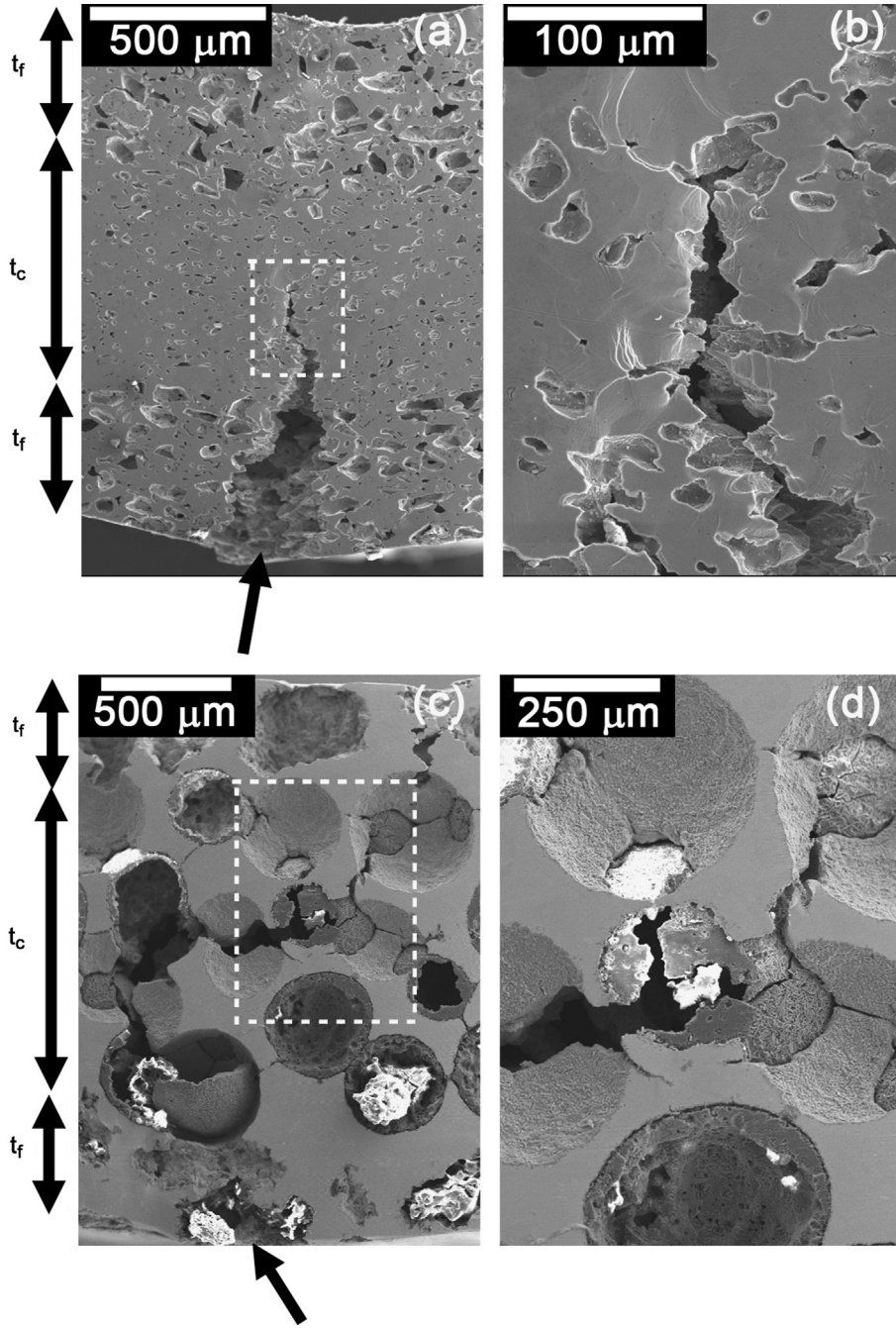


**Fig. 7.** SEM micrographs of tested sandwiches showing crack in porous faces of (a and b) E-Brite [EB-5] and (c and d) J5 sandwich structures [J5-1]. Thickness of facings ( $t_f$ ) and core ( $t_c$ ) are identified. Micrographs (b and d) are magnified views of the core area around the crack tip, in the box highlighted in (a and c). White particles in the lower portion of the J5 images (c and d) are remnants of the alumina polishing slurry. The crack initiation sites at the bottom of the beam are highlighted by an arrow in (a) and (c).

with  $E_c^*$  as Young’s modulus of the core. While most structural sandwiches are designed with thin facings and a compliant core, this study utilizes thick faces and a rigid core; thus the full expression for flexural rigidity is used here without the simplification typically employed, as in Ref. [34]. The yield stress,  $\sigma_y^f$ , of the foam facings was calculated according to the Gibson–Ashby relation:

$$\sigma^* = C_\sigma \sigma_s \left( \frac{\rho^*}{\rho_s} \right)^{3/2} \quad (5)$$

where  $\sigma_s$  is the yield stress of the bulk material, and  $C_\sigma$  a scaling factor (Table 2). The E-Brite core Young’s modulus was calculated according to Eq. (2) resulting in  $E_c^* = 208$  GPa for  $\rho^*/\rho_s = 0.93$ . For the syntactic J5 core, a value of  $E_c^* = 87$  GPa was used [35].

The yield load for each beam, as calculated by Eqs. (3)–(5) and, as measured, are reported in Table 2. As in the case of rigidity, correlated error was determined by taking the standard deviation of face thickness, core thickness, width, span, and relative density measurements and subsequently propagating these through Eqs. (3) and (4). Excluding uncertainty, discrepancies between experimental and calculated values for E-Brite range from 26% to 45% (with respect to experimental values), which are higher than observed by Pollien et al. [14] for graded Al foams, where calculated estimates overpredicted experimental values by ~20%. In part, this may be due to the gradual deviation from linearity beyond the elastic regime, which makes it difficult to ascertain the experimental value of  $P_y$ . As in Ref. [14], the yield load was chosen as the value that coincided with the lowest accurately measurable

**Table 2**  
Constants used in Gibson–Ashby relations (Eqs. (2) and (5)) for determination of stiffness and yield load.

Constant	E-Brite	J5
$C_E$	1.2 [25]	1 [22]
$E_S$ (GPa)	200 [26]	180 [22]
$E_f^*$ (GPa)	61	49
$C_\sigma$	0.7 [25]	1 [22]
$\sigma_s$ (MPa)	345 [26]	367 [22]
$\sigma_{fy}^*$ (MPa)	124	175
$S$ (mm)	16	18

**Table 3**

Calculated and experimental rigidities ( $P/\delta$ ) and yield load ( $P_y$ ) for E-Brite and J5 sandwich structures as calculated according to Eqs. (1)–(5) and as measured experimentally. Standard deviation of the relative density, facing thickness, core thickness, width, and span measurements were computed and the correlated error was determined by propagating through calculations for rigidity and yield load.

Sample	$P/\delta$ [N/mm]		$P_y$ [N]	
	Calculated	Experimental	Calculated	Experimental
EB-1	600 ± 270	718	34 ± 11	57
EB-2	790 ± 330	740	41 ± 11	57
EB-3	930 ± 390	770	41 ± 12	74
EB-4	750 ± 320	843	38 ± 11	66
EB-5	820 ± 340	686	40 ± 11	54
EB-6	750 ± 320	434	38 ± 11	67
EB-7	790 ± 330	715	39 ± 11	67
J5-1	1130 ± 410	769	163 ± 24	77
J5-2	1210 ± 430	601	162 ± 30	58

permanent deflection of 20  $\mu\text{m}$ . Eq. (3) predicts higher yield loads for J5 than for E-Brite sandwiches, but there is a little difference in experimental values between the two types of sandwiches. One possible reason for this is the difference in place-holder size relative to facing thickness. The J5 sandwich likely underperforms as compared to the expected theoretical value due to the fact that the face thickness is smaller than the largest  $\text{NaAlO}_2$  powders. The yield strength of the matrix material is thus likely lower than the predicted value of 175 MPa since the minimum number ( $\sim 7$ ) of the largest features (i.e., pores) are not repeated in the face [2]. Hence, this resulted in unpredictable, premature plastic flow. Also possible is the accumulation of damage in the alumina, which leads to early yield of the J5.

#### 4. Conclusions

Two new manufacturing methods – one based on powder-metallurgy and the other on melt infiltration – are developed to create thin sandwich structures of E-Brite and J5 alloys, respectively. For E-Brite sandwiches with  $\text{NaCl}$  place-holders in the facings (removed in a later step to produce open porosity), good flatness was achieved at the interface between the core and faces. Some residual porosity (6.9%) remained in the core after sintering, but it is well below the percolation limit indicating the core can prevent gas flow between adjacent cells in its application as a SOFC interconnect. In the case of J5, larger place-holders of  $\text{NaAlO}_2$  were used in the facings but good interface flatness was still achieved between the open porosity facings and the syntactic closed-porosity core. These processing routes are general in nature, and allow for alternate place-holders, sizes, volume fractions, and matrix alloys to tailor sandwich structures for a wide range of applications.

Both types of sandwiches, cut into beams with thicknesses ( $\sim 1.4$ – $2.2$  mm) comparable to those of typical SOFC interconnects, demonstrate repeatable mechanical properties in three-point bending tests. Stiffness calculations closely match measured E-Brite beam behavior but overpredict the experimental performance of J5 sandwich beams for the limited number of samples tested. In the case of yield load, calculated values for E-Brite slightly underestimate experimental values, while J5 experimental performance is significantly overestimated. With J5, the discrepancy is likely caused by the fact that the face thickness is smaller than the largest  $\text{NaAlO}_2$  powders in addition to damage accumulation in the alumina hollow spheres in the core.

#### Acknowledgments

The authors thank Dr. R. Bhat (GE Global Research Center) for useful discussions, Dr. N.O. Shanti (NU) for his assistance with thermoreversible gelcasting, M.E. Seniw (NU) and Dr. M. Cox (NU) for assistance with bend testing, and Dr. P.D. Jablonski (National Energy Technology Laboratory; Albany, OR) for providing the J5 ingot. Part of this research was funded by NASA through a subcontract from GE (Award NNC06CB31C). JAS also thanks Bell Labs, the National Science Foundation, and the Northwestern University Nanoscale Science & Engineering Center for graduate research fellowships.

#### References

- [1] L.-P. Lefebvre, J. Banhart, D.C. Dunand, *Adv. Eng. Mater.* 10 (2008) 775.
- [2] L.J. Gibson, M.F. Ashby, *Cellular Solids: Structure and Properties*, Cambridge University Press, Cambridge, 1997.
- [3] H.-P. Degischer, B. Kriszt, *Handbook of Cellular Metals: Production, Processing, Applications*, Wiley-VCH, Weinheim, 2002.
- [4] J. Banhart, *Prog. Mater. Sci.* 46 (2001) 559.
- [5] A.G. Evans, J.W. Hutchinson, M.F. Ashby, *Prog. Mater. Sci.* 43 (1998) 171.
- [6] H.N. Wadley, *Philos. Trans. A Math. Phys. Eng. Sci.* 364 (2006) 31.
- [7] M.F. Ashby, *Metal Foams: A Design Guide*, Butterworth-Heinemann, Boston, 2000.
- [8] E. Magnucka-Blandzi, K. Magnucki, *Thin Wall Struct.* 45 (2007) 432.
- [9] J. Hohe, W. Becker, *Appl. Mech. Rev.* 55 (2002) 61.
- [10] C.A. Steeves, N.A. Fleck, *Int. J. Mech. Sci.* 46 (2004) 561.
- [11] T.M. McCormack, R. Miller, O. Kesler, L.J. Gibson, *Int. J. Solids Struct.* 38 (2001) 4901.
- [12] O. Kesler, L.J. Gibson, *Mater. Sci. Eng. A Struct.* 326 (2002) 228.
- [13] Y. Conde, A. Pollien, A. Mortensen, *Scr. Mater.* 54 (2006) 539.
- [14] A. Pollien, Y. Conde, L. Pambaguian, A. Mortensen, *Mater. Sci. Eng. A Struct.* 404 (2005) 9.
- [15] J.W. Fergus, *Mater. Sci. Eng. A Struct.* 397 (2005) 271.
- [16] M.C. Tucker, *J. Power Sources* 195 (2010) 4570.
- [17] Z. Yang, K.S. Weil, D.M. Paxton, J.W. Stevenson, *J. Electrochem. Soc.* 150 (2003) A1188.
- [18] N.Q. Minh, *Solid State Ionics* 174 (2004) 271.
- [19] J.D. Carter, T.A. Cruse, J.-M. Bae, J.M. Ralph, Deborah J. Myers, R. Kumar, M. Krumpelt, *Mater. Res. Soc. Symp.* (2003) 756.
- [20] S. Molin, M. Gazda, B. Kusz, P. Jasinski, *J. Eur. Ceram. Soc.* 29 (2009) 757.
- [21] S. Molin, B. Kusz, M. Gazda, P. Jasinski, *J. Power Sources* 181 (2008) 31.
- [22] Y. Boonyongmaneerat, D.C. Dunand, *Adv. Eng. Mater.* 10 (2008) 379.
- [23] Y. Boonyongmaneerat, D.C. Dunand, *Acta Mater.* 57 (2009) 1373.
- [24] K.A. Erk, D.C. Dunand, K.R. Shull, *Acta Mater.* 56 (2008) 5147.
- [25] J.A. Scott, D.C. Dunand, *Acta Mater.* 58 (2010) 6125.
- [26] E-Brite Alloy for Solid Oxide Fuel Cells, Technical Data Blue Sheet, Allegheny Ludlum, 2002.
- [27] M.E. Seitz, W.R. Burghardt, K.T. Faber, K.R. Shull, *Macromolecules* 40 (2007) 1218.
- [28] N.O. Shanti, D.B. Hovis, M.E. Seitz, J.K. Montgomery, D.M. Baskin, K.T. Faber, *Int. J. Appl. Ceram. Technol.* 6 (2009) 593.
- [29] P.D. Jablonski, D.E. Alman, *Int. J. Hydrogen Energy* 32 (2007) 3705.
- [30] ASTM D7249, ASTM International, West Conshohocken, PA, 2006.
- [31] Y.B. Matus, L.C. De Jonghe, C.P. Jacobson, S.J. Visco, *Solid State Ionics* 176 (2005) 443.
- [32] L.J. Gibson, *Mater. Sci. Eng. A Struct.* 110 (1989) 1.
- [33] L.J. Gibson, *Mater. Sci. Eng. A Struct.* 67 (1984) 125.
- [34] T.C. Triantafillou, L.J. Gibson, *Mater. Sci. Eng. A Struct.* 95 (1987) 37.
- [35] Y. Boonyongmaneerat, Personal Communication, 2010.